LA-UR -81-2135

CONF-810810--16

TITLE: RADIATION-INDUCED TRANSIENT ABSORPTION IN OPTICAL FIBERS

MASTER

AUTHOR(S): L. D. Looney, p-14
G. Turquet de Beaurecard, P-14
P. B. Lyons, P-14
R. E. Kelly, P-14

SUBMITTED TO: 25th Annual Technical Symposium
SPIE Technical Programs Committee
San Diego, CA

August 24-28, 1981

University of California

LOS ALAMOS SCIENTIFIC LABORATORY
Post Office Box 1663 Los Alamos, New Mexico 87545
An Affirmative Action/Equal Opportunity Employer

Form No. 836 R3
St. No. 2629
12/78

UNITED STATES
DEPARTMENT OF ENERGY
CONTRACT W-7405-ENG 36

SUBMITTED

Radiation-Induced Transient Absorption in Optical Fibers

L.D. Looney, G. Turquet de Beauregard, P.B. Lyons, R.E. Kelly

Los Alamos National Laboratory, P.O. Box 1663, MS 410, Los Alamos, NM 87545

Abstract

Transient absorption in optical fibers has been studied with emphasis on fast absorption components. Radiation damage was induced with a Febetron 706 electron accelerator, modified to deliver an electron pulse width of 1.1 ns. Dye lasers were synchronized to the accelerator to provide a light pulse through the fiber during the radiation pulse. The output light pulse was detected with a biplanar vacuum photodiode. Four scope traces were used on each electron pulse to monitor the Febetron output, the input drive pulse, and two records of the output pulse on two sweep speeds. Detailed data were acquired for times less than 100 ns after irradiation. An insulated enclosure was used to vary fiber temperature from -30°C to +250°C. Several fibers were studied with emphasis on ITT T303 PCS fiber. Data were acquired at 600 and 850 nm. Theoretical modeling of the data will be presented.

Introduction

Most previous studies of radiation-induced transient absorption in optical fibers have concentrated on times 100 ns (or longer) after irradiation.[1-3] Only a few studies have explored the time regime below 100 ns[4,5]. The research reported herein summarizes transient absorption on selected optical fibers with ~1 ns resolution.

Experimental configuration

The experimental apparatus is shown in Fig. 1. A Chromatix CMX-4 flashlamp-pumped laser with rhodamine dye provided a 1 μs 600 nm light pulse. For some tests an optical parametric oscillator shifted the wavelength to 850 nm. The resulting laser pulses showed significant noise and a long (200 m) length of low bandwidth (~20 MHz-Km) plastic-clad-silica (PCS) fiber was used to reduce the bandwidth of the signal presented to the radiation environment. One photodiode monitored the laser output and triggered a Febetron 706 electron accelerator. A second diode monitored the pulse shape exiting the 200 m fiber (light was stripped from the PCS fiber with a sharp bend over the diode). A Tektronix 7844 monitored both the second diode and a third diode viewing the output of the total system with 20 ns/div sweep speed. A Tektronix 7104 oscilloscope recorded prompt data with 2 ns/div sweep speed.

The fiber under test was spliced to the 200 m PCS fiber and routed across a 2.5 cm diameter exposure port. In most cases, no more than 2 m of the test fiber extended from the test region to a splice to 20 m of Corning SDF fiber (>20 MHz-Km). The SDF fiber was routed into a screen room and recorded on the third high speed photodiode. This last diode was filtered to the probe wavelength.

The time response of the final diode and Tektronix 7104 was about 500 ps FWHM. The Febetron 706 provides a 3 ns FWHM under standard operating conditions. However, the Febetron 706 electron energy spectrum changes with time (from a 600 keV end point) and most of the pulse tail consists of slow electrons. By filtering the electrons with 103 mg/cm^2 of Al the pulse width (as measured on a fast, 4 GHz, Faraday cup with the Tektronix 7104 scope) was 1.1 ns FWHM (cf. Fig. 2). The energy loss in the aluminum was about 160 keV.

An insulated enclosure allowed temperature variations from about -40°C (where some PCS samples became extremely attenuating) to 250°C (where the cladding of some PCS samples was charred). Temperature was monitored to ±2°C.

Dosimetry with a low energy electron beam is very difficult. Approximate dose was determined with radiochromic films[6] that were filtered with thin glass or aluminum plates to approximate dose within the fiber. Dose averaged 700 kRad at the center of a 125 μm diameter silica fiber. Dose varied significantly with depth in the fiber (±20%). (Accurate dosimetry should use a higher electron energy with a more constant depth-dose profile. However, higher energy flash electron machines provide much slower pulse outputs.) Shot-to-shot reproducibility of dose was about ±25%. Diameters (of the glass portion) of tested fibers ranged from 125 to 300 μm. Absolute calibration of the dosimeter film has not been attempted att Los Alamos. Manufacturer's data show no dose rate or dose limitations of the film up to the levels used here. Manufacturer's data are used for absolute dose values.

Typical raw data are shown in Fig. 3 for ITT T303 PCS (Suprasil core) fiber. The data were acquired at 600 nm wavelength and two temperatures. At lower temperatures, attenuation is much more pronounced and recovers very slowly.

The length of exposed fiber was varied in 2.5 cm increments. Depending on the observed loss, more or less fiber was required to obtain high quality data. At early times where loss is maximum, only 2.5 cm were exposed. At late times and high temperatures up to 25 cm of fiber were exposed. Data quality was degraded when small attenuations were studied under these latter conditions. With multiple lengths of exposed fiber, care was taken to assure that each fiber was not shielded by a neighboring fiber.

Measurements

Effort was concentrated on the ITT T303 PCS fiber that has been shown to have less short-term transient attenuation than most other tested fibers.[5] This fiber was studied at 600 and 850 nm with a wide temperature range and a large number of shots. Only data from unirradiated fiber was accepted, although up to 10 multiple shots did not change the measurements significantly (for times to 100 ns). Average data are plotted in Figs. 4 and 5. Within experimental uncertainty of ±15%, the observed peak attenuation at 155°C and 215°C for an 850 nm wavelength were equal. Significantly less attenuation is observed at 850 nm and at elevated temperatures.

In an effort to study dependence of these data on total dose, the aluminum absorber was increased to reduce the dose significantly. Dosimetry was not attempted at this low dose as uncertainty would have been very large. The absorber was increased until peak attenuation was reduced by one decade. The data of Fig. 6 show identical attenuation pulse shapes for the two, widely differing, dose levels.

A limited study of several other fibers was made at 850 nm and room temperature. Figure 7 collects these data for the indicated fibers. With exception of three fibers, these are all PCS fibers. The three exceptions have pure silica cores with doped cladding. For this experimental series only, the aluminum beam filter was reduced to 67 mg/cm^2 to offset a degraded dose output from the Febetron 706. Pulse width of the e-beam changed (increased) by <0.5 ns over the data of Fig. 2. Depth-dose data were acquired for this case. The data for each fiber were corrected to a dose (1.4 mRad) at the fiber center equivalent to that at the center of the 125 μm T303 fiber. This correction assumed that damage was proportional to dose over the range of the corrections. The thickest fiber, with 300 μm outer silica diameter, required a 25% correction for this effect.

Analysis

The damage and subsequent recovery of an optical fiber exposed to a radiation pulse depends upon a number of factors, not all of which are quantitatively understood. The more important parameters are pulse duration, dose, nature and energy of the radiation (neutrons, gammas, fission fragments, etc.), temperature, fiber composition, and purity. Other factors such as dose rate during the pulse and the pre-existing solid state defects (dislocations, color centers, etc.) probably also affect the response to radiation. In addition, optical attenuation is wavelength dependent.

Many mechanisms have been identified as contributing to transient attenuation in optical fibers. Some of these mechanisms can involve complicated trapping and tunneling phenomena[1,2] At the early times of interest here, however, other mechanisms may dominate.

During the radiation pulse, the energy of the incident electrons is dissipated in, predominantly, ionization and excitation of lattice atoms. The resulting electrons and ions will recombine under the influence of their Coulomb attraction. The speed of this recombination will be governed by the diffusion rate in the lattice. This phenomena in which pairs of electrons and ions recombine is called geminate recombination and has been studied in a variety of materials. On a longer time scale, those electrons which do not recombine very quickly with their geminate "parent" ion may encounter a trap in the lattice. The radiation-induced attenuation of a material will be proportional to the defect concentration, thus the transient absorption should follow the same response as the ion pair concentration.

Based upon geminate recombination theory,[2,7] the (radiation induced) attenuation, for a radiation pulse at t = 0, should follow

$$\beta = \beta_0 e^{\lambda t} \operatorname{erfc} \sqrt{\lambda t} \quad , \tag{1}$$

where β and β_0 are the attenuation coefficients at time t and t = 0, respectively. λ is a measure of the recombination rate and is related to the diffusion constant. The complementary error function is defined as

$$\text{erfc } x = 1 - \text{erf } x = 1 - \frac{2}{\sqrt{\pi}} \int_0^x e^{-u^2}\, du = \frac{2}{\sqrt{\pi}} \int_x^\infty e^{-u^2}\, du \quad . \tag{2}$$

Note that λ determines the decay rate, and from diffusion theory it should vary as

$$\lambda = \lambda_0 \exp(-\varepsilon/kT) \quad , \tag{3}$$

where ε is the barrier height for diffusion. Values of ε for silicate glasses of 0.2-0.4 eV are suggested in some studies[8] while Mattern, et al.[2] found 0.45 eV for germanium-doped silica.

While the emphasis here is on recovery after termination of the pulse, there will be some recovery during the pulse, which will tend to decrease the peak transient absorption to a value below what it would attain if no recovery mechanism occurred. Thus, the peak transient absorption for a given fiber should be a function of dose, pulse length and shape, and temperature.

To test this model, the Febetron 706 data were used to determine a value of λ. For the Febetron, the dose rate was assumed to follow the electron pulse I(t). I(t) was taken from Fig. 2 and normalized to unity. Then the observed attenuation $\beta'(t)$ becomes

$$\beta'(t) = k \int_0^\infty I(t')\, e^{\lambda(t-t')}\, \text{erfc}\, \sqrt{\lambda(t-t')}\, dt' \quad . \tag{4}$$

Two adjustable parameters, λ and k, are then available.

The value of λ in Eq. (4) obviously plays the major role in determining the observed attenuation coefficient at any given time. To investigate this effect, Fig. 8 was constructed for a large range of λ values. In Fig. 8 the geminate recombination function β from Eq. (1) was calculated. These functions were then convolved with the Febetron current pulse, as in Eq. (4), and the resulting $\beta'(t)$ values are shown in Fig. 9. In these calculations, it is implicitly assumed that defect generation rate is proportional to fiber dose rate. It is certainly possible, and even probable, that some classes of defects saturate early in the pulse history. It should be noted that for $\lambda t \gg 1$, $\beta \approx \beta_0/\sqrt{\pi\lambda t}$.

The data for the ITT T303 from Figs. 4 and 5 were compared to the geminate recombination curves of Fig. 9. For each temperature, the value of λ was selected for a best fit and β' was plotted in Figs. 10 and 11. The functional dependence of transient absorption on time is very insensitive to the value of λ, particularly for large values of λ. The chosen values of λ do, however, provide very credible fits at late times. At early times, the fits are very poor.

The values of β_0 at the two wavelengths are different to achieve the fits of Figs. 10 and 11. At 600 nm, β_0 = 200 db/m. At 800 nm, β_0 = ____ db/m.

If the geminate recombination model is correct, for at least later times, the values of λ should be described by equation (3). In Fig. 12, λ is plotted versus 1/T. The fit to the anticipated straight line is quite accurate. Data for both 600 nm and 850 nm fit the same curve. Thus ε is independent of wavelength as should be anticipated.

Geminate recombination does not describe early time behaviour. In Fig. 13, the differences between observed data and the geminate predictions are plotted. At each wavelength a similar difference curve is obtained. This excercise requires small differences between large numbers and is subject to further uncertainties from the ±25% in e-beam dose delivered to the fiber on various shots. Still, the similarity of these difference curves to a single pulse shape is striking. While the peak value of the difference curves is a function of wavelength (~110 db/m at 600 nm and ~37 db/m at 850 nm), it does not demonstrate temperature dependence. The curves appear to be exponential at late times (after the pulse) with a decay constant of ~1/2.2 ns^{-1}.

The other fibers presented in Fig. 7 do not show absorption shapes equivalent to the T303 fiber. Detailed analysis of these other shapes has not been attempted. However, several interesting features may be noted. Three different PCS fibers (ITT T303, QPC QSF-UV, and QPC QSF-A) are markedly different. The QSF-UV, according to the vendor, is designed for better UV properties, and it closely compares to the T303 performance. The QSF-A is inferior to the QSF-UV. It should be noted that a single batch of both T303 and QSF-UV were used to obtain these data, different batches could offer different performance.

The three all-silica fibers are the best such fibers ever tested at Los Aalmos. They are the first all-silica fibers to rival PCS in radiation hardness at short times. The QSF-AS with 300 ppm OHM is indistinguishable from QSF-UV. Furthermore, the "quasi-step" Times Fiber demonstrates impressive radiation resistance while offering 50 MHz-Km bandwidth.

Several hypotheses for the temperature independent component can be suggested. Much of the electron energy will be deposited in localized regions of small dimensions (spur regions). Within these regions, effective lattice temperatures will be far higher than the bulk material. Diffusion in these regions may be governed by this effective temperature and the result recombination would appear to be unaffected by the bulk material temperature. Stated differently, spur ion densitities may be so high that initial recombination does not follow the geminate model. Another hypothesis would suggest that excited electronic states of the constituent atoms are present and are decaying with a characteristic decay time of 2 ns. Other explanations are possible, but must be consistent with the temperature independence of this prompt component.

Conclusion

Geminate recombination provides a good description of transient attenuation in very high purity silica fibers (like ITT T303) for times to 100 ns over a wide temperature range, but only if a second component of attenuation is postulated. This second, temperature independent, component of attenuation approximately demonstrates an exponential decay with a 0.4 ns^{-1} decay constant. The geminate model requires lattice activation energy of 0.22 eV for high purity PCS fibers. Geminate recombination is diffusion-controlled and therefore is strongly temperature dependent.

The two attenuation components display different wavelength dependence. The geminate term decreases by 5x between 600 and 850 nm while the "exponential" term decreases by 3x.

Several other fiber types, consisting of other PCS fibers and all-glass step index fibers with silica cores, demonstrate an attenuation which is larger than the T303 observations. The differences are much more evident at late times. However, one all-glass fiber, QSF-AS with 300 ppm OH, demonstrated performance close to the T303 fiber and is the best all-glass fiber tested at Los Alamos to date. If degraded purity accounts for differences between the various fibers, one can speculate whether T303 has achieved optimal purity. The fit of geminate recombination theory to T303 data suggests that T303 may be close to the optimum.

References

1. E. J. Friebele, G. H. Sigel, Jr., M. E. Gingerich, "Radiation-Induced Optical Absorption Spectra of Fiber Optic Waveguides in the 0.4-1.7 μm Region," in Fiber Optics ed. by B. Bendow and S. S. Mitra, Plenum Press (1979, New York) p. 355, and E. J. Friebele, Optical Engineering 18 (1979) p. 552.
2. P. L. Mattern, L. M. Watkins, C. D. Skoog, and E. H. Barsis, IEEE Trans. Nuc. Sic. NS-22 (1975) p. 2468.
3. C. D. Skoog, "A Summary of Radiation-Induced Transient Absorption and Recovery in Fiber Optic Waveguides," Sandia Lab Report SAND 76-8056 (Nov. 1976).
4. P. Zagarino, C. H. Lin, M. A. Nelson, T.J. Davies, N. J. Norris, and J. W. Ogle, "Radiation Response Measurement of Fibers in the Picosecond Region," presented at Symposium on Fiber Optics in the Nuclear Environment, Proceedings published by Defense Nuclear Agency, DNA-5308P-2, March 1980, p. 118.
5. P. B. Lyons, R. E. Kelly, L. D. Looney, "Short-Term Radiation Effects in Optical Fibers," presented at Symposium on Fiber Optics in the Nuclear Environment, Proceedings published by Defense Nuclear Agency, DNA-5308P-2, March 1980, p. 83.
6. Obtained from Far West Technology, Goleta, CA.
7. S. J. Rzad, P. P. Infelta, J. M. Warman, and R. H. Schuler, Jrnl. Chem. Phys. 52 (1970) p. 3971.
8. A. Barkatt, M. Ottolenghi, and J. Rabani, Jrnl. Phys. Chem 77 (1973), p. 2857.

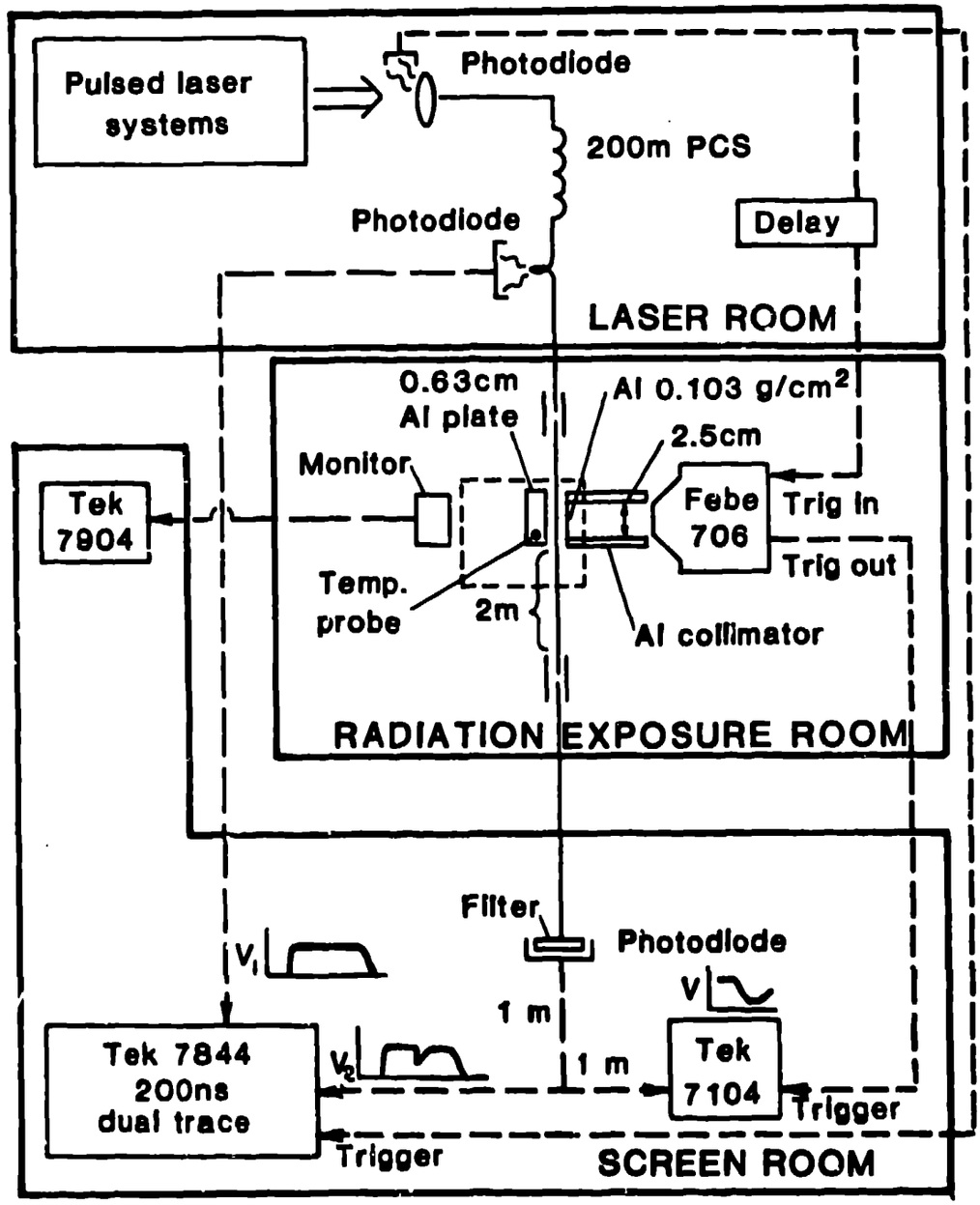

Fig. 1. Schematic of experimental apparatus. Fiber splices were made with vee grooves or with micro-positioners.

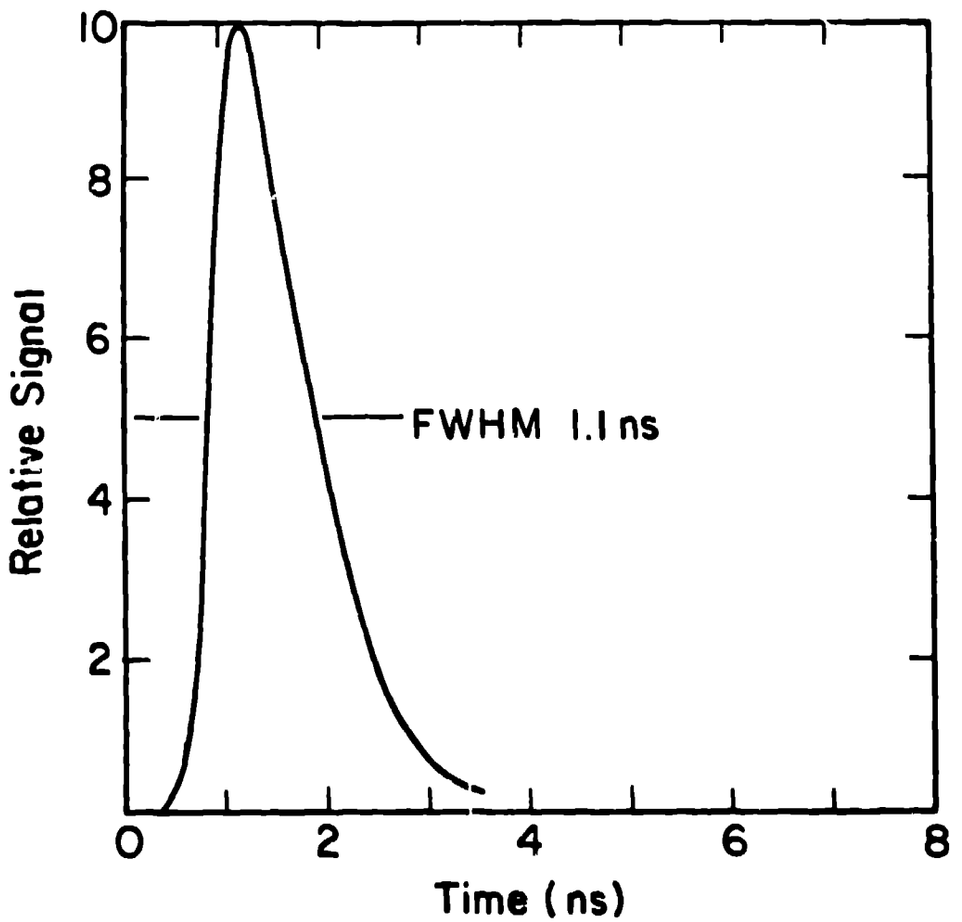

Fig. 2. Current vs. time for the Febetron 706 electron beam after filtration by 103 mg/cm^2 aluminum.

ITT T303 FIBER
WAVELENGTH 600nm DOSE 250 KRAD

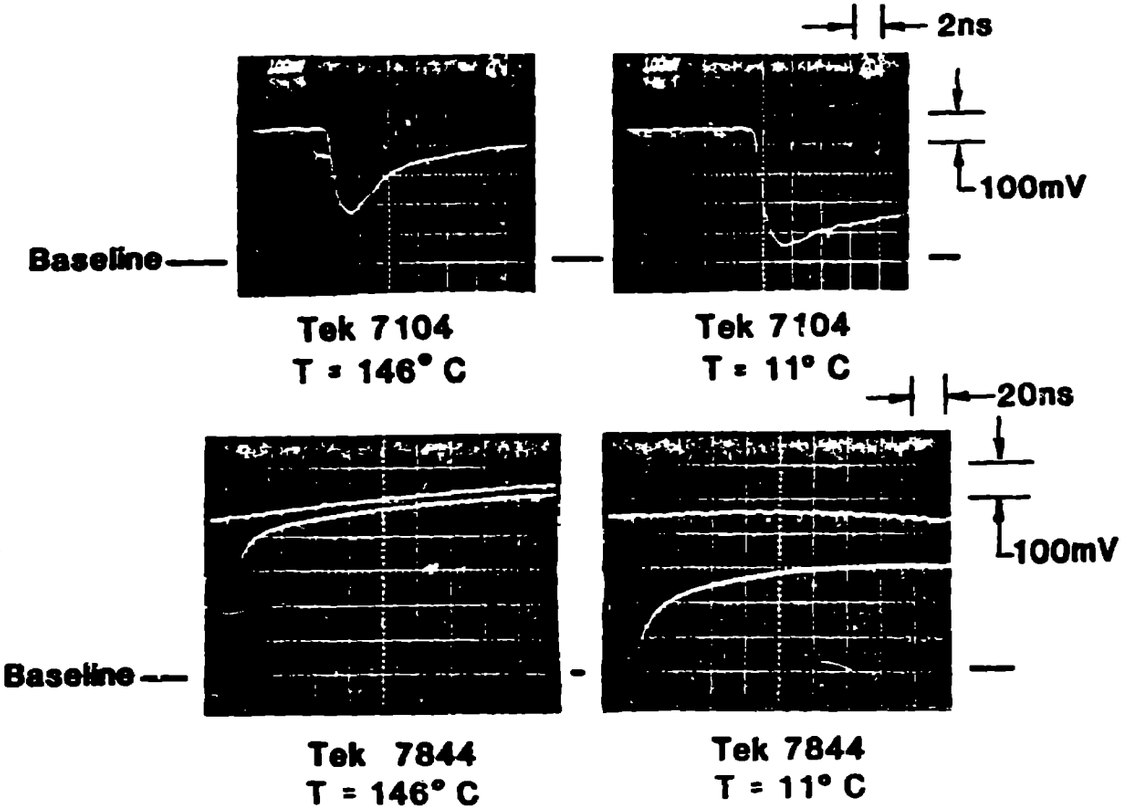

Fig. 3. Typical pulse shapes for ITT T303 fiber. Wavelength was 600 nm. Dose was 700 KRad.

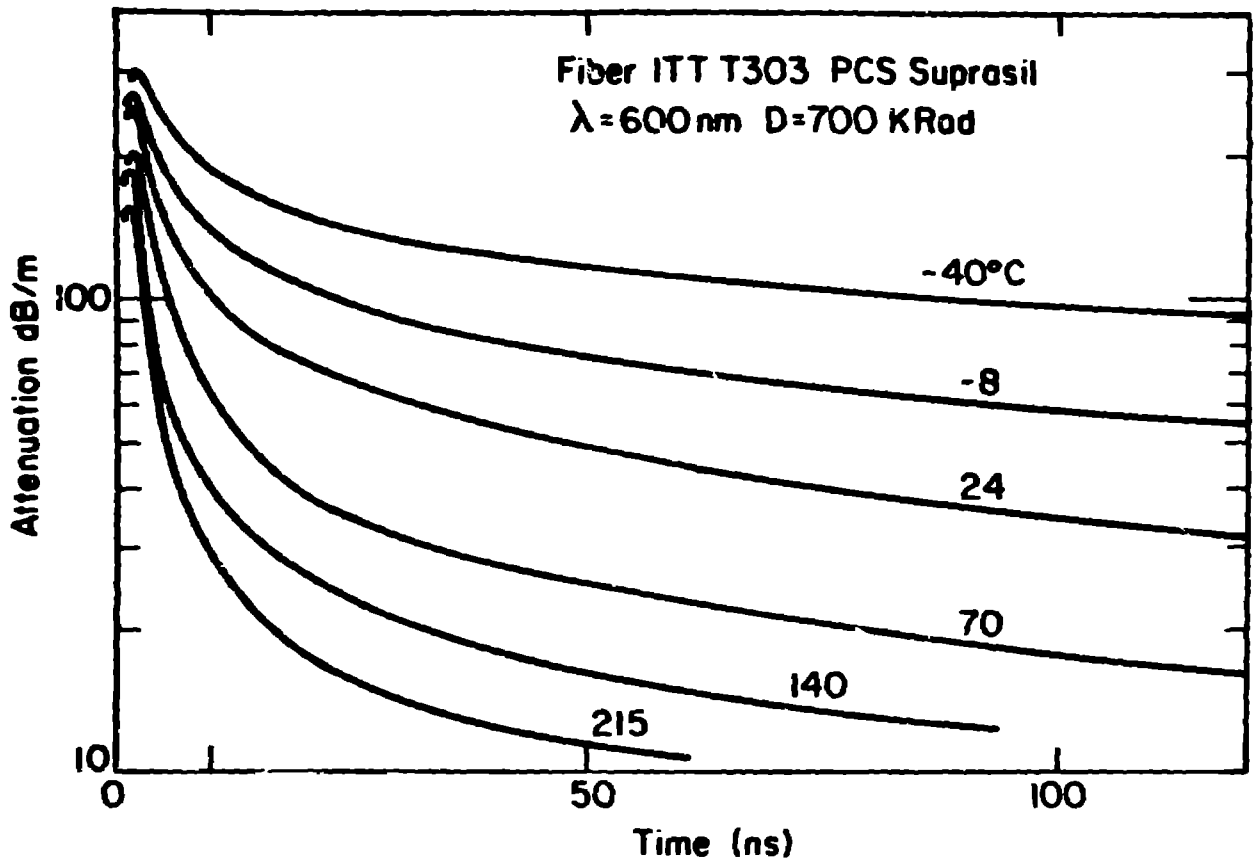

Fig. 4. Experimental transient absorption recovery data for ITT T303 fiber at 600 nm wavelength.

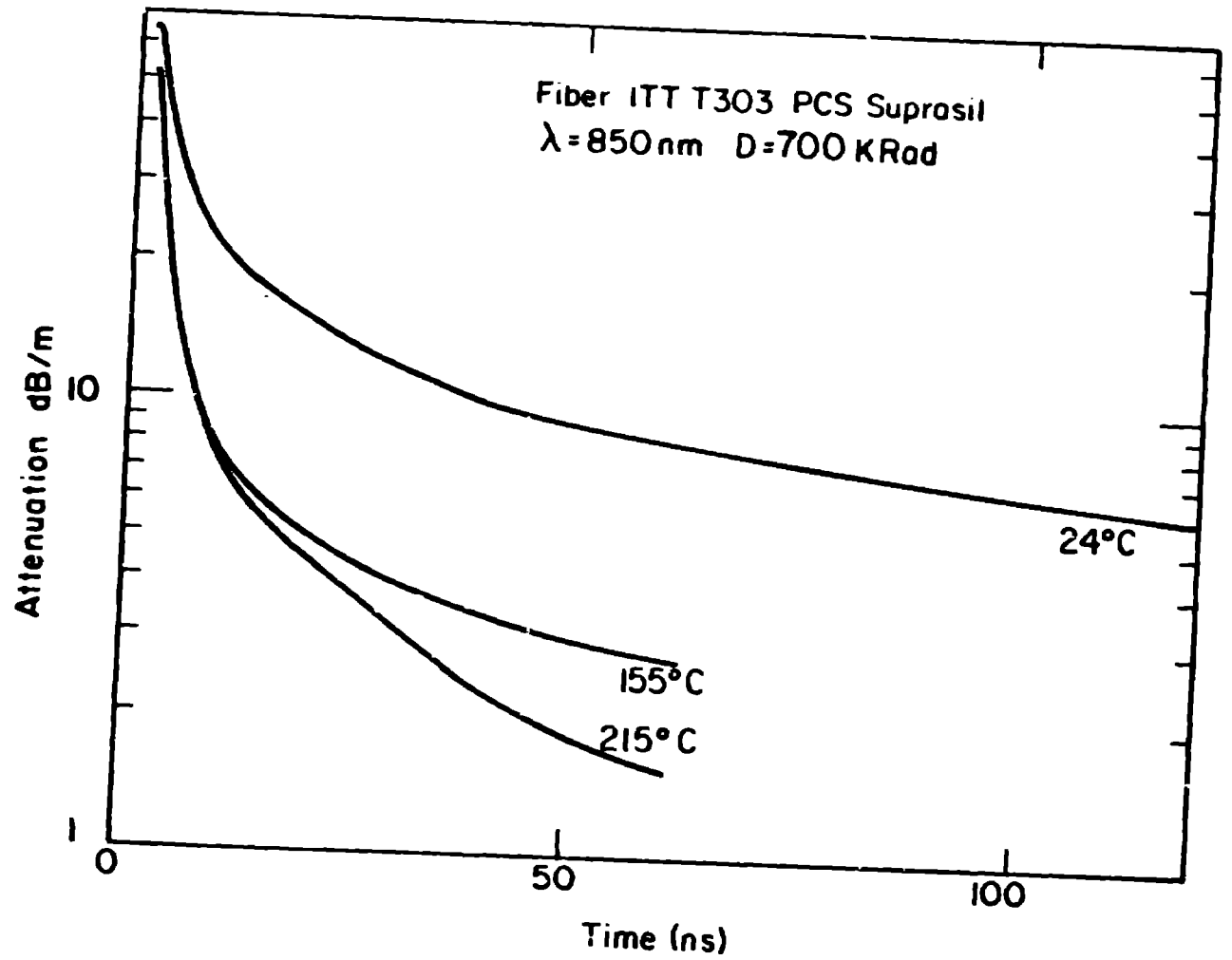

Fig. 5. Experimental transient absorption recovery data for ITT T303 fiber at 850 nm wavelength.

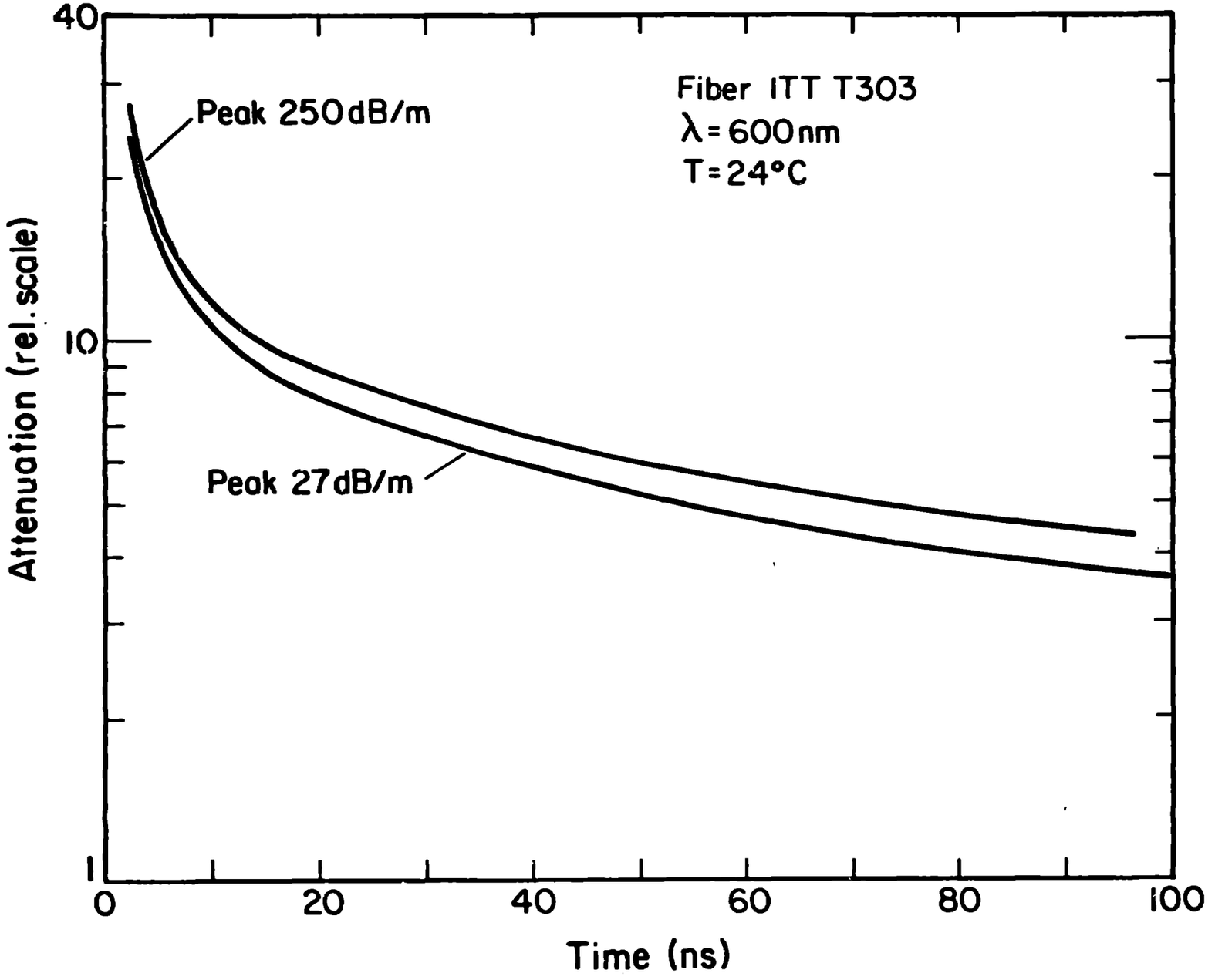

Fig. 6. Comparison of T303 transient absorption recovery for two dose levels.

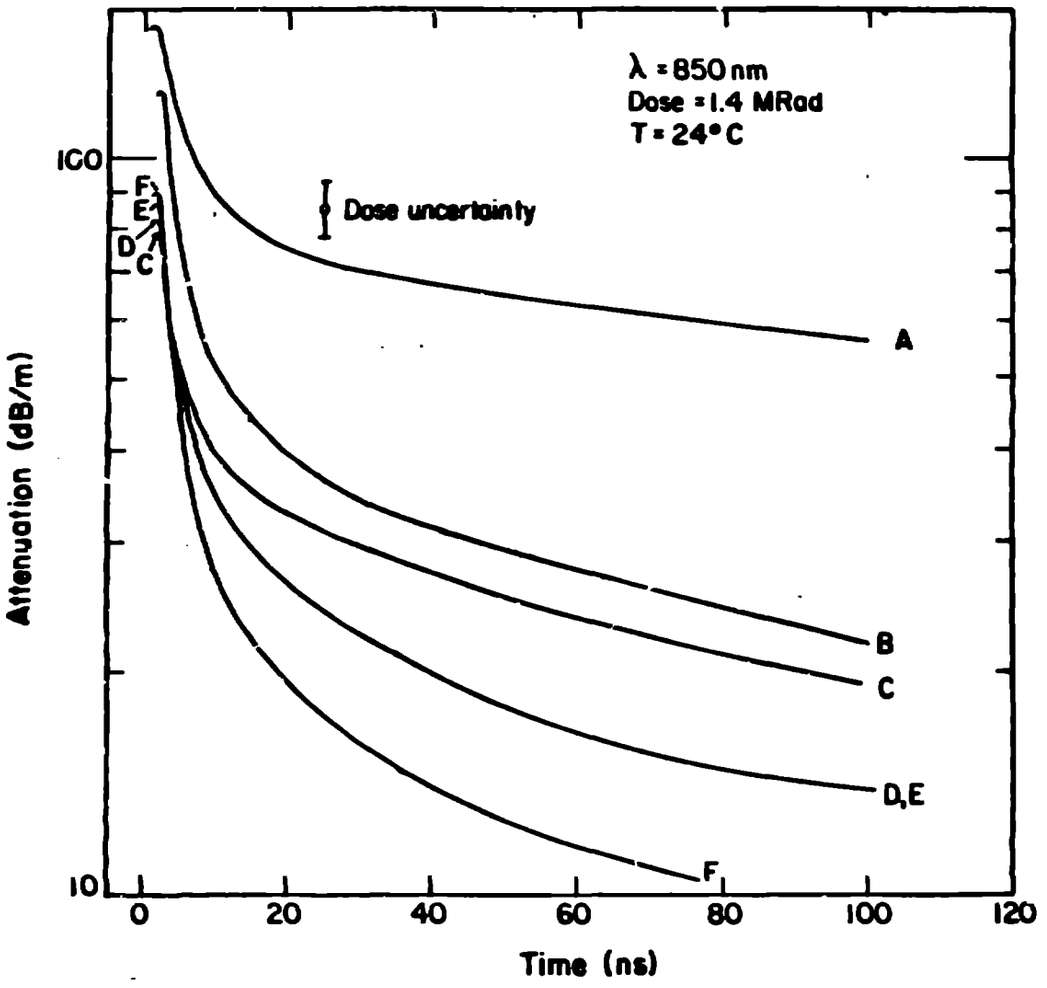

Fig. 7. Experimental transient absorption data for six fibers at 850 nm wavelength, room temperature, and about 1.4 MRad dose. Fibers are

A. Times Fiber Communications quasi-step fiber, 200/250 μm core/clad, boron-doped cladding, 50 MHz-Km bandwidth
B. Quartz Products Corp. QSF-A, 125 μm core PCS
C. Quartz Products Corp. QSF-AS, 200/300 μm core/clad, fluorine-doped cladding, 30 ppm OH, 30 MHz-Km bandwidth
D. Quartz Products Corp. QSF-AS, 200/300 μm core/clad, fluorine-doped cladding, 300 ppm OH, 20 MHz-Km bandwidth
E. Quartz Products Corp. QSF-UV, 200 μm core PCS, ~20 MHz-Km
F. ITT T303 125 μm Suprsil core PCS

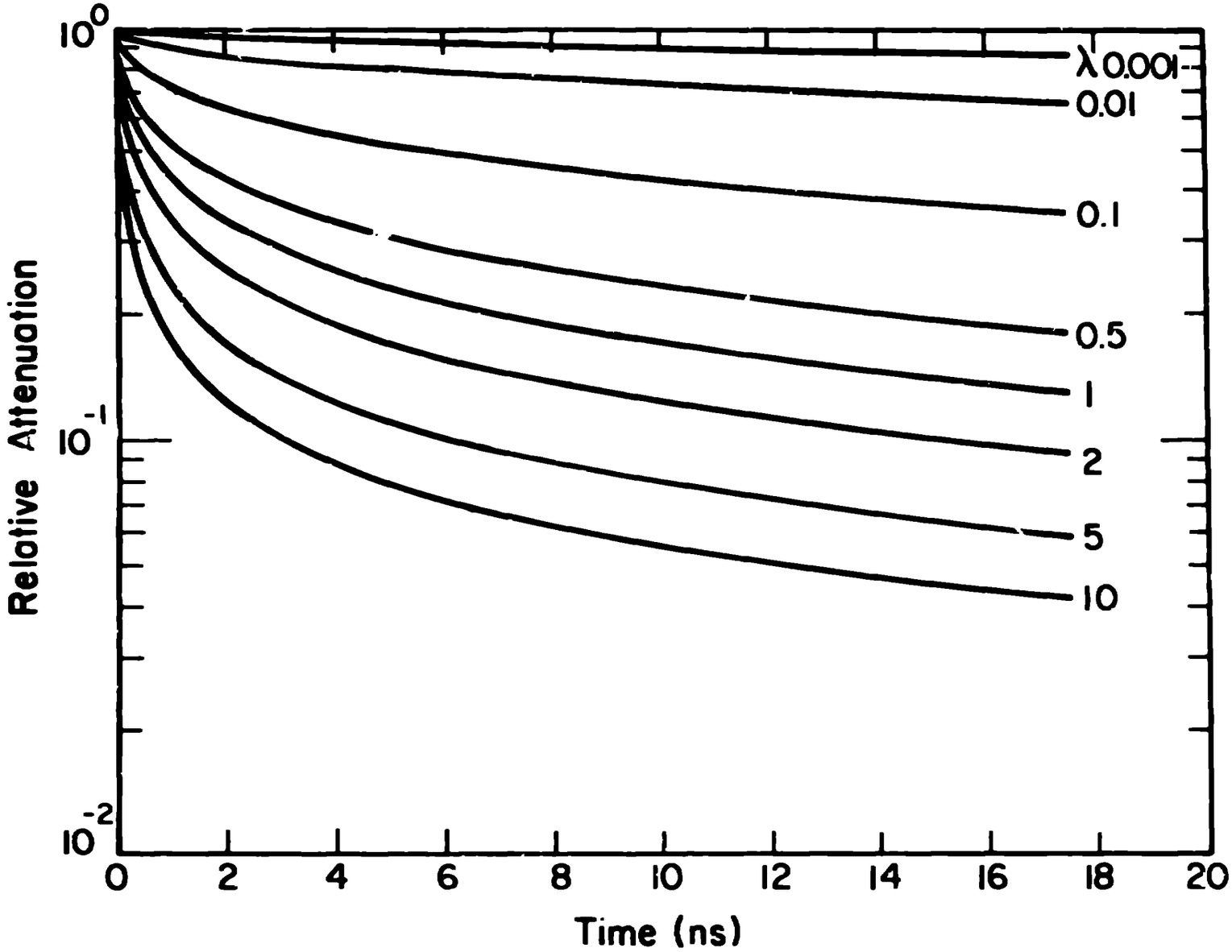

Fig. 8. Geminate recombination function, $\cdot = e^{\cdot t}$ erfc $\sqrt{\cdot t}$, in ns^{-1}.

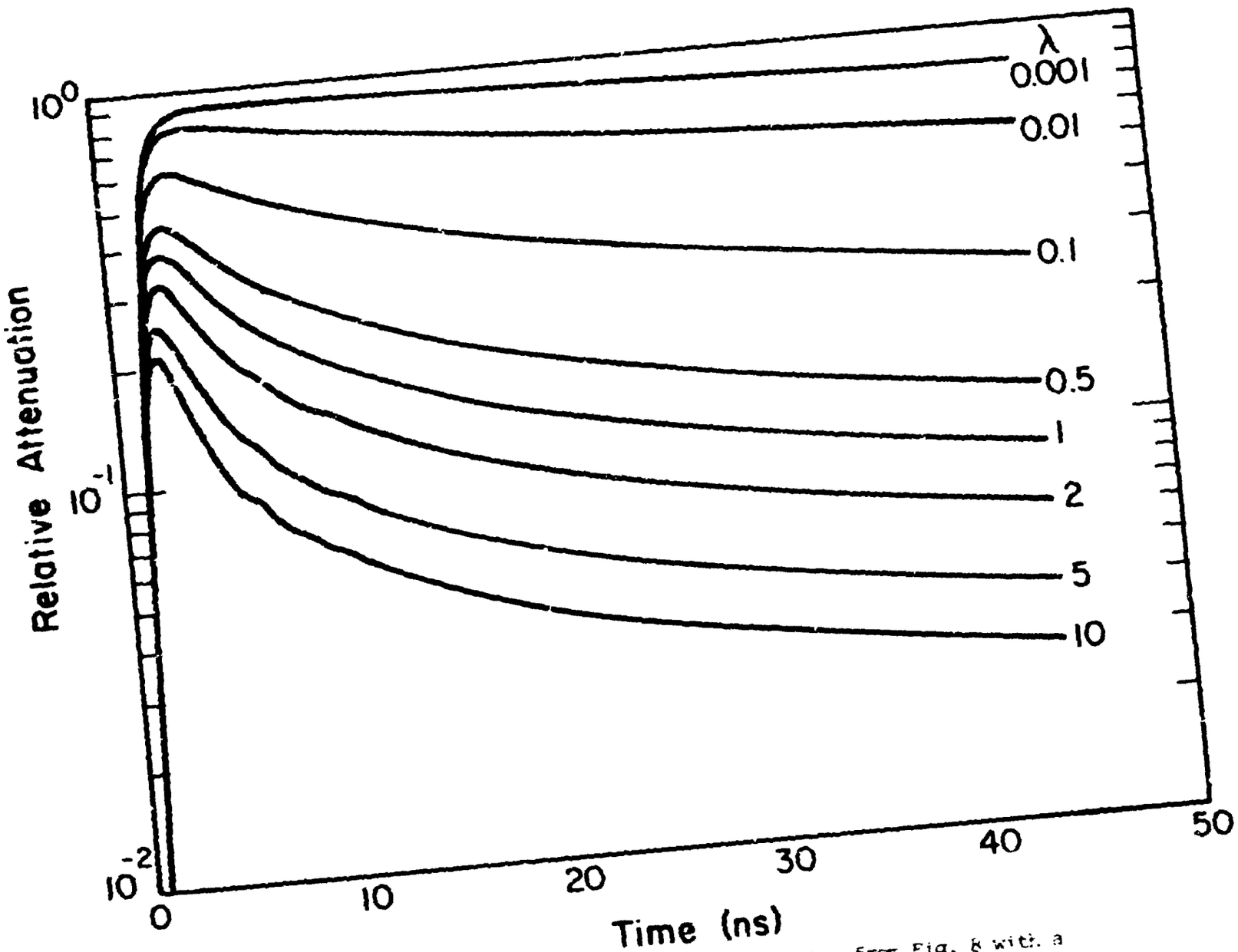

Fig. 9. Convolution of geminate recombination function from Fig. 8 with a normalized Febetron current pulse (Fig. 2), $\cdot$ 15 ns^{-1}.

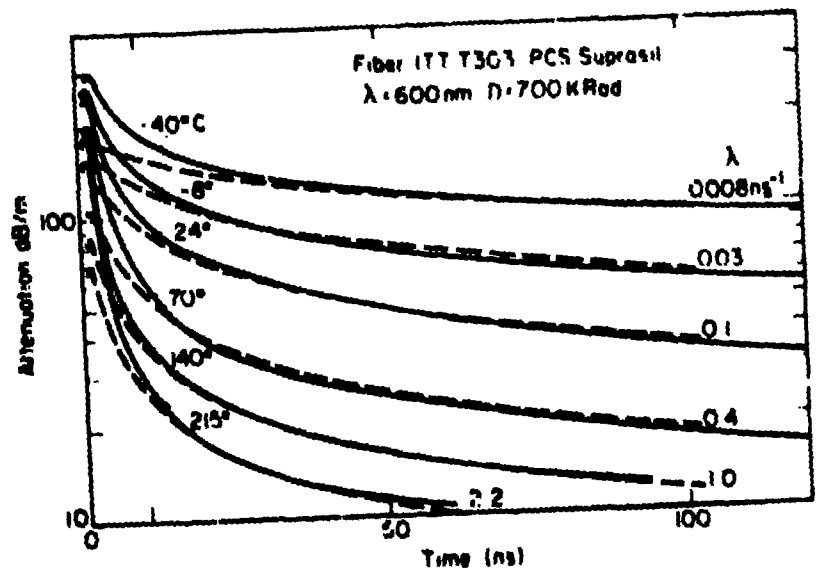

Fig. 10. Comparison of "least fit" convolved gaussian curves from Fig. 9 with experimental data for T303 fiber at 600 nm.

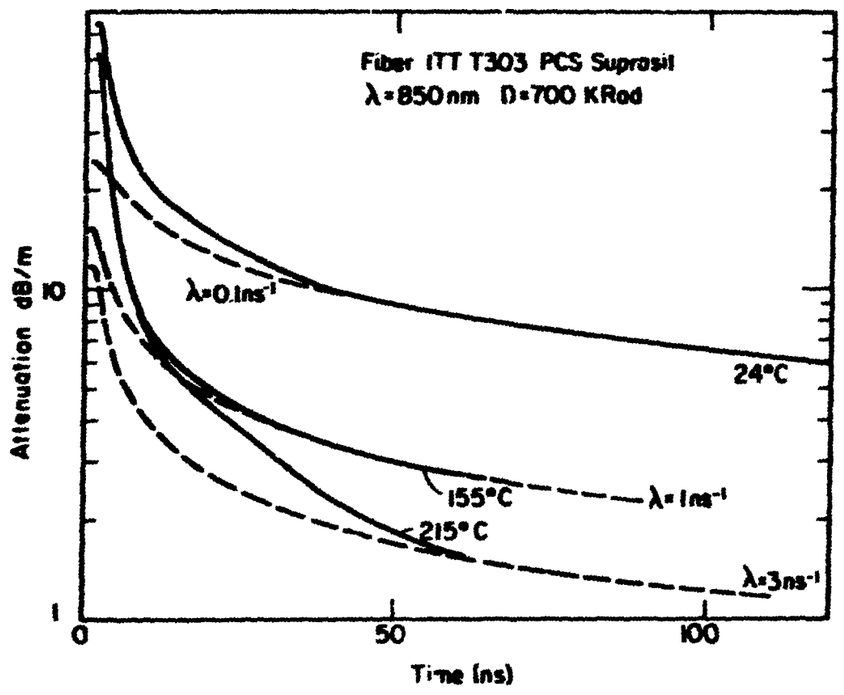

Fig. 11. Comparison of "best fit" convolved germinate curves from Fig. 9 with experimental data for T303 fiber at 850 nm.

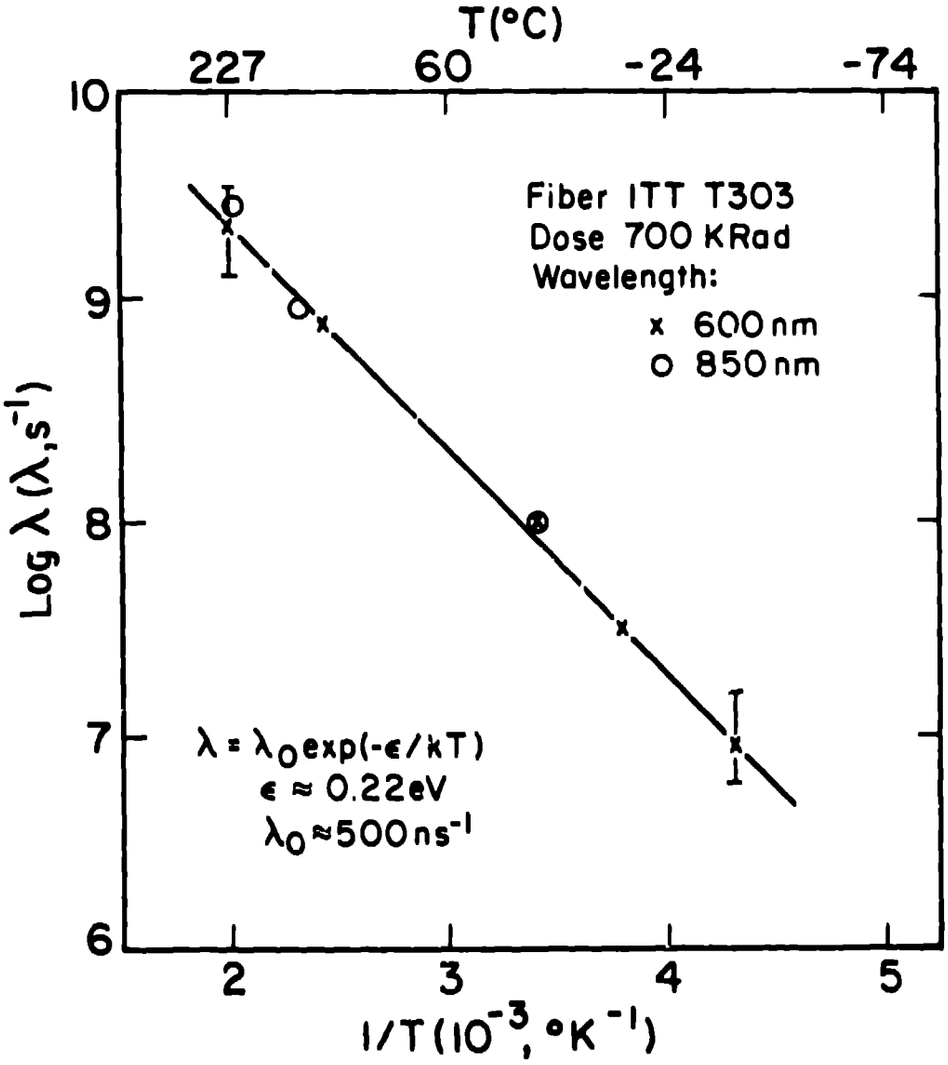

Fig. 12. Arrhenius plot of temperature dependence of the fiber recovery parameter λ.

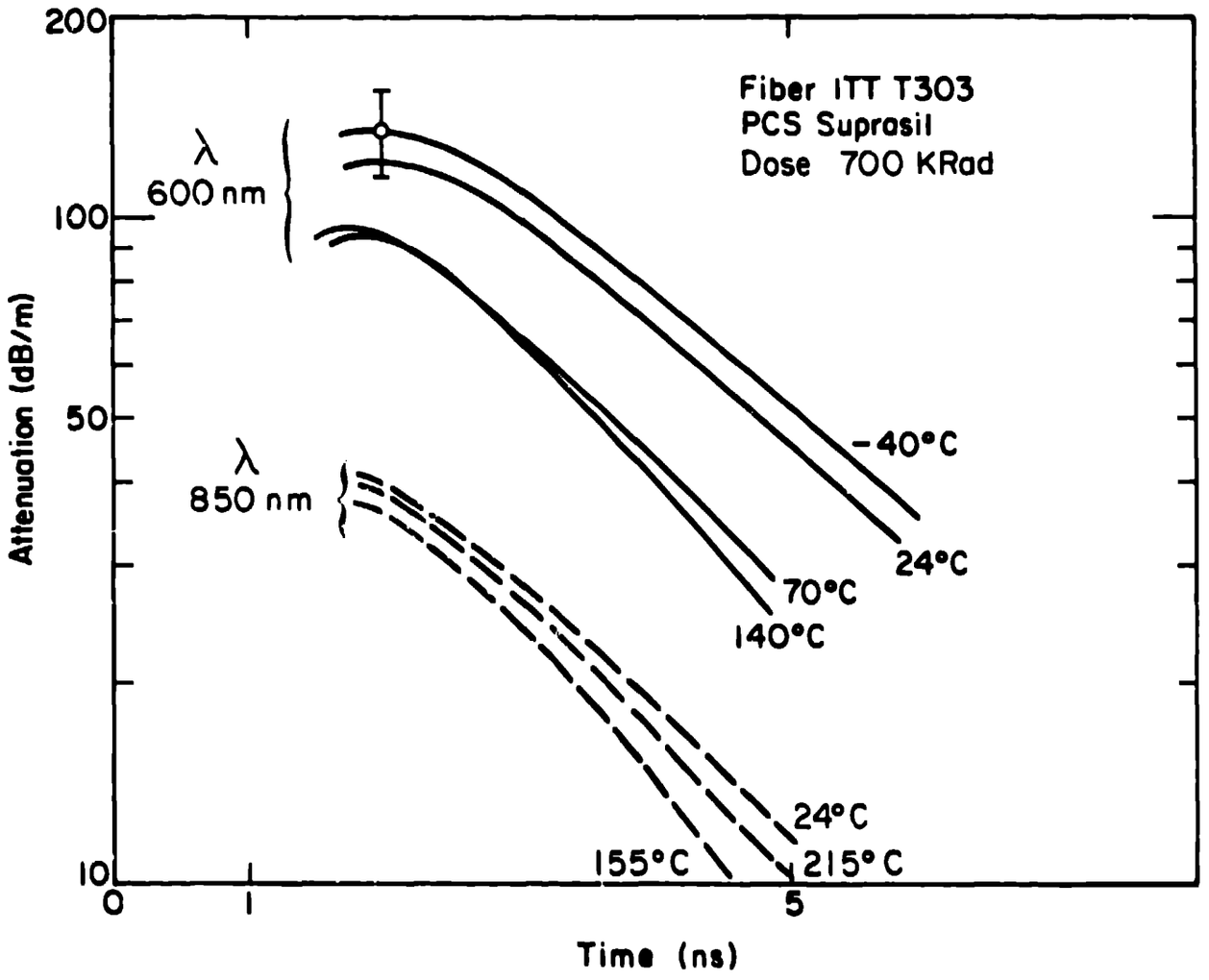

Fig. 13. Plot of difference between T303 experimental data and the geminate recombination model.